Journal of Nonlinear Dynamics and Applications
http://dx.doi.org/10.62762/JNDA.2026.569839

RESEARCH ARTICLE

The Return Map in the Class $\mathcal{O}_C$: Geometry, Dynamics, and Thickness Regularity

Mohammed Barkatou[1] and **Mohamed El Morsalani**[2,*]

[1] ISTM Laboratory, Chouaib Doukkali University, El Jadida 24000, Morocco
[2] QWave Consult, Ostfildern, Germany

Abstract

We study a geometrically defined return map associated with domains in the class $\mathcal{O}_C$, where a fixed convex core $C \subset \mathbb{R}^N$ is linked to the outer boundary $\partial\Omega$ through outward normal rays and a thickness function $d : \partial C \to (0, \infty)$. The radial map $\Phi(c) = c + d(c)\nu(c)$ is combined with a reciprocal map that follows the inward normal to $\partial\Omega$ back to its first intersection with the convex core. Their composition $F = \pi \circ \Phi : \partial C \to \partial C$ defines a geometrically generated discrete dynamical system on ∂C. Using the exact normal geometry of the radial parametrization, we derive the local quadratic-remainder formula $F(c)-c = d(c)\big(I-d(c)S_c\big)^{-1}\nabla_{\partial C}d(c)+O\big(|\nabla_{\partial C}d(c)|^2\big)$, where S_c is the shape operator of ∂C. Thus curvature enters the leading-order dynamics through a positive anisotropic preconditioning of the thickness gradient. At points where the relevant derivatives exist, fixed points of the return map coincide with critical points of the thickness function. Under additional smoothness assumptions, we obtain the linearization $DF(c_*) = I + d_*\big(I - d_*S_*\big)^{-1}H_*$, with H_* the Hessian operator of d at c_*. This yields a local stability classification governed jointly by thickness variation and curvature. The analytical results are validated by exact unit-circle computations. We also establish regularity transfer between the thickness function and the outer boundary and derive global bi-Lipschitz bounds for the radial parametrization from convex metric projection. These results provide a geometric foundation for the study of boundary-induced discrete dynamics generated by normal interactions.

Keywords: return map, geometric dynamics, thickness function, convex geometry, normal parametrization, curvature-preconditioned dynamics, discrete dynamical systems, bi-Lipschitz maps.

1 Introduction

Geometric properties of domain boundaries play a central role in convex geometry, shape analysis, and geometric dynamical systems. Among the basic structures involved are normal parametrizations, metric projections, curvature operators, and the regularity of offset or parallel boundaries [1]. These ideas also arise naturally in shape optimization, where geometric information carried by the boundary is used to describe admissible variations and associated dynamical processes; see, for example, [2–5].

Submitted: 28 May 2026
Revised: 16 September 2026
Accepted: 17 September 2026
Published: 23 September 2026

Vol. 2, **No.** 3, 2026.
10.62762/JNDA.2026.569839

***Corresponding author:**
Mohamed El Morsalani
mohamed.elmorsalani@qwave-consult.eu

Citation
Barkatou, M., & El Morsalani, M. (2026). The Return Map in the Class $\mathcal{O}_C$: Geometry, Dynamics, and Thickness Regularity. *Journal of Nonlinear Dynamics and Applications*, 2(3), 192–216.

A related point of view arises in the geometric-normal framework introduced by Barkatou [6]. In this setting, a fixed convex set $C \subset \mathbb{R}^N$ is contained in a larger domain Ω, and the geometry of the two boundaries is linked through normal rays. For the subclass $\mathcal{O}_C$ considered here, every point $c \in \partial C$ determines a unique point of the outer boundary along the outward normal to the convex core. This gives the radial representation

$$\Phi(c) = c + d(c)\nu(c),$$

where $\nu(c)$ is the outward unit normal to ∂C and $d : \partial C \to (0, \infty)$ is the associated thickness function.

Normal parametrizations of convex geometries and their curvature properties continue to play an important role in current geometric analysis. Recent work includes normal-coordinate descriptions of strictly convex bodies and offset geometries [7], structural results for sets of positive reach [8], and generalized curvature measures associated with normal geometry [9]. Related developments in shape analysis emphasize the differential geometry of admissible domains and shape spaces [4, 5]. Gradient-type iterations on embedded submanifolds, in which the choice of Riemannian metric acts as a preconditioner, are treated systematically in Riemannian optimization [10]. This provides a natural setting in which to read the curvature-preconditioned gradient step that arises from the normal geometry considered in the present paper.

A central motivation for studying this construction is that it provides a direct passage from static boundary geometry to a geometrically generated discrete dynamics. The return map is not imposed as an external numerical scheme, optimization algorithm, or prescribed flow. It is generated by the geometry itself: the two boundary shapes, their normal fields, and the thickness separating them determine the iteration. Consequently, three objects that are usually studied separately become linked within a single construction: the geometry of the admissible domain, the scalar thickness landscape on ∂C, and a discrete dynamical system on the convex-core boundary.

This interaction is already visible at first order. The thickness gradient does not act alone; it is transformed by the curvature-dependent operator

$$d(c)\big(I - d(c)S_c\big)^{-1}.$$

Thus local motion records simultaneously how the thickness varies and how the underlying convex boundary bends. This provides a natural mechanism by which geometric information is converted into dynamical information. More broadly, it raises the possibility of studying normal interactions between nested or constrained boundaries through dynamical methods, and conversely of extracting geometric information from the resulting dynamics. Establishing this mechanism rigorously is therefore a natural first step before addressing its global dynamical, variational, or topological consequences.

The mechanism studied here is generated directly by the geometry of the two boundaries. Starting from $c \in \partial C$, one first moves along the outward normal of the convex core to

$$x = \Phi(c) \in \partial\Omega \setminus C.$$

From x, one then follows the inward normal to $\partial\Omega$ until it meets the convex core for the first time. If

$$\pi : \partial\Omega \setminus C \longrightarrow \partial C$$

denotes this reciprocal map, the composition

$$F = \pi \circ \Phi : \partial C \longrightarrow \partial C$$

defines a discrete return map. Thus one iteration is the geometric round-trip

$$c \longmapsto \Phi(c) \longmapsto F(c).$$

The two legs are governed by different normal fields: the first by the outward normal to ∂C, and the second by the inward normal to $\partial\Omega$. Their interaction is the source of the nontrivial return dynamics.

The first objective of the paper is to derive the local structure of this map directly from the geometry. With the convention

$$S_c = -D\nu(c)\big|_{T_c\partial C}$$

for the shape operator of the convex core, the differential of the radial map naturally introduces the positive tangential operator

$$I - d(c)S_c.$$

The resulting first-order expansion of the return map near a critical point of the thickness is

$$F(c) - c = d(c)\big(I - d(c)S_c\big)^{-1}\nabla_{\partial C} d(c) + O\big(|\nabla_{\partial C} d(c)|^2\big).$$

The leading term is therefore not an ordinary gradient step. Instead, the tangential gradient of the thickness is modified by the curvature-dependent operator

$$B_c = d(c)\big(I - d(c)S_c\big)^{-1}.$$

In principal directions of the convex core, its eigenvalues are

$$\frac{d(c)}{1 + d(c)\kappa_i(c)},$$

so the curvature of ∂C enters explicitly and anisotropically into the local displacement.

A second objective is to identify the equilibrium structure associated with this geometry. We show that, at points where the relevant derivatives exist,

$$F(c) = c \quad \Longleftrightarrow \quad \nabla_{\partial C} d(c) = 0.$$

Under stronger local smoothness assumptions, the derivative of the return map at a critical point c_* is

$$DF(c_*) = I + B_* H_*,$$

where

$$B_* = d_*\big(I - d_* S_*\big)^{-1}$$

and H_* is the Hessian operator of the thickness function at c_*. Since B_* is positive definite, the spectrum of the linearization can be expressed through the self-adjoint operator

$$B_*^{1/2} H_* B_*^{1/2}.$$

This yields a local stability classification in which the second-order geometry of the thickness and the curvature of the convex core enter simultaneously.

The analytical formulas are complemented by exact computations for a unit-circle core. In that case the geometric return can be evaluated explicitly, allowing the first-order displacement and the local multiplier to be checked directly from the normal construction rather than from the asymptotic formula itself. These examples are used as numerical validation of the local theory.

The radial representation also has consequences independently of the dynamics. We establish regularity transfer between the thickness function and the outer boundary under the appropriate transversality assumptions. Moreover, since the inverse radial map is the restriction of the metric projection onto the closed convex set C, its non-expansiveness gives the global lower estimate

$$|c_1 - c_2| \le |\Phi(c_1) - \Phi(c_2)|.$$

Together with the Lipschitz regularity of d and of the normal field, this yields global bi-Lipschitz control of the radial parametrization without a perturbative smallness condition.

The purpose of the present work is to establish these geometric and local dynamical foundations. Questions concerning global orbit structure, Lyapunov or monotonicity properties, nontrivial periodic behaviour, continuous-time limits, and topological constraints on the equilibrium structure require additional hypotheses and are left for separate investigation.

The paper is organized as follows. Section 2 introduces the geometric setting, the convex core, and the class $\mathcal{O}_C$, and establishes radial accessibility. Section 3 defines the thickness function and the radial parametrization. Section 4 introduces the reciprocal map and the geometric round-trip, while Section 5 formulates the induced discrete return dynamics and its exact closure relations. Section 6 derives the first-order expansion and discusses its geometric interpretation, including circle and sphere consistency checks. Section 7 characterizes the fixed points, derives the linearization, and studies local stability. Section 8 provides numerical validation using the exact unit-circle return map. Section 9 establishes the regularity and bi-Lipschitz properties of the radial parametrization. Section 10 discusses the scope of the construction and directions for further study, and Section 11 concludes the paper.

2 Geometric Setting and the Class $\mathcal{O}_C$

2.1 Ambient Space and Notation

Let $N \ge 2$ and let $\mathbb{R}^N$ be endowed with the Euclidean inner product $\langle \cdot, \cdot \rangle$ and norm $|\cdot|$. For a set $A \subset \mathbb{R}^N$, we denote by ∂A and $\mathrm{int}(A)$ its boundary and interior, respectively.

Throughout the paper, $C \subset \mathbb{R}^N$ denotes the fixed convex core. At a regular point $c \in \partial C$, the symbol $\nu(c)$ denotes the *outward* unit normal to ∂C. For $x \in \partial\Omega \setminus C$, the symbol $n(x)$ denotes the *inward* unit normal to $\partial\Omega$ whenever it exists. Thus the two normal fields have opposite geometric roles and will not be denoted by the same symbol.

The metric projection onto the closed convex set C is denoted by

$$P_C : \mathbb{R}^N \longrightarrow C.$$

For $x \notin C$, the projection $P_C(x)$ is unique.

If ∂C is differentiable at c, we use the sign convention

$$S_c = -D\nu(c)\big|_{T_c\partial C}$$

for the shape operator; see, e.g., [11]. Hence, for a convex hypersurface with outward normal, the eigenvalues of S_c are $-\kappa_i(c)$, where $\kappa_i(c) \geq 0$ are the usual principal curvatures. In particular,

$$I - d(c)S_c$$

has eigenvalues $1 + d(c)\kappa_i(c) > 0$ whenever $d(c) \geq 0$.

Tangential gradient and Hessian on ∂C are denoted by

$$\nabla_{\partial C} d \qquad \text{and} \qquad \mathrm{Hess}_{\partial C}\, d,$$

respectively.

2.2 The Convex Core C

Let $C \subset \mathbb{R}^N$ be a compact convex set with nonempty interior. Throughout the dynamical part of the paper we assume that ∂C is of class $C^{1,1}$. Consequently, the outward unit normal field

$$\nu : \partial C \longrightarrow \mathbb{S}^{N-1}$$

is well defined and Lipschitz continuous.

For $c \in \partial C$, let

$$N_C(c) = \{\xi \in \mathbb{R}^N : \langle \xi, z - c\rangle \leq 0 \quad \text{for every } z \in C\}$$

denote the normal cone of C at c. This is the vector form of the normal cone used in the geometric-normal framework of Barkatou [6]. Since ∂C is C^1, the normal cone is one-dimensional:

$$N_C(c) = \{r\nu(c) : r \geq 0\}.$$

Convexity also implies that the metric projection

$$P_C : \mathbb{R}^N \longrightarrow C$$

is uniquely defined and non-expansive; see, e.g., [12]. For $x \notin C$ and $c \in \partial C$,

$$c = P_C(x) \quad \Longleftrightarrow \quad x - c \in N_C(c).$$

Hence, under the present regularity assumption,

$$c = P_C(x) \Longleftrightarrow x = c + r\nu(c) \quad \text{for some } r > 0. \tag{1}$$

Thus every point outside C lies on a unique outward normal ray issued from its metric projection onto ∂C.

Since ∂C is $C^{1,1}$, the derivative $D\nu$ exists almost everywhere on ∂C and is essentially bounded. With the sign convention fixed in Section 2.1,

$$S_c = -D\nu(c)\big|_{T_c\partial C}$$

is therefore defined almost everywhere. If $\kappa_1(c), \ldots, \kappa_{N-1}(c) \geq 0$ denote the usual principal curvatures of the convex hypersurface at such a point, then the eigenvalues of S_c are

$$-\kappa_1(c), \ldots, -\kappa_{N-1}(c).$$

2.3 The Geometric Normal Property

We recall the geometric normal property introduced by Barkatou [6]. Let

$$\mathcal{N}_\Omega = \{x \in \partial\Omega : n(x) \text{ exists}\}$$

denote the set of regular boundary points of Ω, where $n(x)$ is the inward unit normal introduced in Section 2.1.

Since ∂C is of class $C^{1,1}$, the selected normal of Barkatou's general formulation is uniquely determined at every $c \in \partial C$. We therefore define the outward half-normal

$$\Delta_c^+ = \{c + r\nu(c) : r \geq 0\}, \tag{2}$$

and the selected normal line

$$\ell_c = \{c + r\nu(c) : r \in \mathbb{R}\}.$$

Definition 2.1 (C-geometric normal property)**.** An open set $\Omega \subset \mathbb{R}^N$ is said to satisfy the C-geometric normal property, abbreviated C-GNP, if the following conditions hold:

(P1) $\mathrm{int}(C) \subset \Omega$;

(P2) $\partial\Omega$ is Lipschitz outside C;

(P3) for every $x \in \mathcal{N}_\Omega \setminus C$, the inward normal half-line

$$\{x + t\, n(x) : t \geq 0\}$$

intersects C;

(P4) for every $c \in \partial C$, the set $\ell_c \cap \Omega$ is connected.

The formulation above is the specialization of the original definition in [6] to a convex core with $C^{1,1}$ boundary. In particular, the C-GNP is a geometric condition and does not by itself impose the differentiability required later for the return-map analysis.

We shall use the following consequence of Barkatou's geometric theory [6]. If Ω satisfies the C-GNP, then every outward half-normal Δ_c^+ intersects $\partial\Omega$ in at most one point. Equivalently,

$$\#(\Delta_c^+ \cap \partial\Omega) \leq 1, \qquad c \in \partial C. \tag{3}$$

This follows from the separation characterization of the C-GNP and the associated uniqueness result for half-lines contained in the normal cone [6].

2.4 The Class $\mathcal{O}_C$

We now specify the subclass of C-GNP domains on which the return dynamics will be defined. The additional assumptions below are not part of the original C-GNP of Barkatou; they provide the regularity and radial accessibility required for the differential analysis of the return map.

Definition 2.2. Let $C \subset \mathbb{R}^N$ be the compact convex core introduced above. The class $\mathcal{O}_C$ consists of open sets $\Omega \subset \mathbb{R}^N$ satisfying the following conditions:

(O1) Ω satisfies the C-geometric normal property;

(O2) $\partial\Omega \setminus C$ is an orientable hypersurface of class $C^{1,1}$;

(O3) for every $c \in \partial C$, the outward normal half-line Δ_c^+ defined in (2) intersects $\partial\Omega \setminus C$;

(O4) this intersection is transverse.

By (3), condition (O3) determines a unique point of $\partial\Omega$ on each outward normal ray. We denote this point by

$$\Phi(c) = c + d(c)\nu(c), \qquad c \in \partial C, \tag{4}$$

where $d(c) > 0$ is the corresponding radial distance.

The transversality condition in (O4) means that the normal ray is not tangent to $\partial\Omega$ at $\Phi(c)$. At points where the inward unit normal $n(\Phi(c))$ is defined, this is equivalent to

$$\langle n(\Phi(c)), \nu(c)\rangle \neq 0. \tag{5}$$

Thus $\mathcal{O}_C$ is a regular subclass of the C-GNP geometry for which every point of ∂C admits a well-defined outward radial link to the outer boundary.

2.5 Radial Accessibility

The preceding assumptions imply that the outer boundary is globally accessible from ∂C along the outward normal rays. The key point is that this statement follows from convex projection and does not require the inward normal from $\partial\Omega$ to terminate at the metric projection.

Proposition 2.3 (Radial accessibility). *Let $\Omega \in \mathcal{O}_C$. Then for every $x \in \partial\Omega \setminus C$ there exists a unique $c \in \partial C$ and a unique $r > 0$ such that*

$$x = c + r\nu(c). \tag{6}$$

Moreover,

$$c = P_C(x). \tag{7}$$

Consequently, the radial map

$$\Phi : \partial C \longrightarrow \partial\Omega \setminus C$$

defined in (4) is bijective and satisfies

$$\Phi^{-1} = P_C|_{\partial\Omega\setminus C}. \tag{8}$$

Proof. Let $x \in \partial\Omega \setminus C$ and set

$$c = P_C(x).$$

Since C is closed and convex, the metric projection is uniquely defined. Because $x \notin C$, one has $c \in \partial C$. By (1),

$$x = c + r\nu(c)$$

for some $r > 0$. Thus x belongs to the outward normal half-line Δ_c^+.

By condition (O3), Δ_c^+ meets $\partial\Omega \setminus C$, while (3) shows that it can meet $\partial\Omega$ in at most one point. Hence this point must be $x = \Phi(c)$.

The uniqueness of c follows from the uniqueness of the metric projection onto the convex set C, and then $r = |x - c|$ is also unique. Therefore Φ is bijective, and (8) follows. □

Remark 2.4. Since the metric projection onto a closed convex set is non-expansive, Proposition 2.3 yields

$$|c_1 - c_2| \le |\Phi(c_1) - \Phi(c_2)| \qquad \text{for all } c_1, c_2 \in \partial C. \tag{9}$$

This estimate will be used in Section 9 to obtain the lower bi-Lipschitz bound without a smallness assumption.

3 Thickness Function and Radial Parametrization

3.1 Definition of the Thickness Function

Let $\Omega \in \mathcal{O}_C$. By Proposition 2.3, for every $c \in \partial C$ there exists a unique point of $\partial\Omega \setminus C$ on the outward normal ray issued from c. We denote the corresponding distance by

$$d(c) > 0.$$

Equivalently, $d : \partial C \to (0, \infty)$ is characterized by

$$\Phi(c) = c + d(c)\nu(c) \in \partial\Omega \setminus C, \qquad c \in \partial C. \tag{10}$$

We call d the *thickness function* of Ω relative to the convex core C.

Since

$$c = P_C(\Phi(c))$$

by Proposition 2.3, the thickness also admits the geometric representation

$$d(c) = |\Phi(c) - c| = \operatorname{dist}\big(\Phi(c), C\big). \tag{11}$$

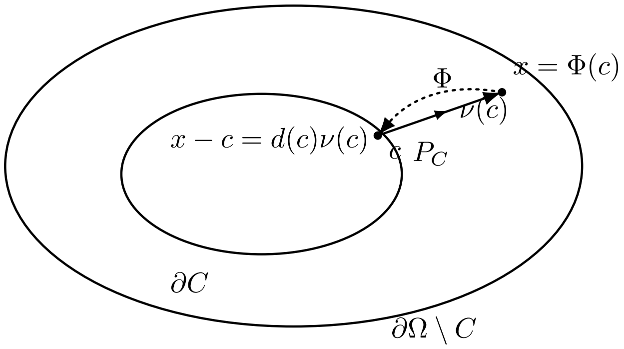

Figure 1. Radial parametrization of the outer boundary. For each $c \in \partial C$, the radial map sends c to the unique point $x = \Phi(c) \in \partial\Omega \setminus C$ lying on the outward normal ray. The metric projection of x onto the convex core is $P_C(x) = c$. The sketch is schematic.

Thus $d(c)$ measures the distance from the convex core to the outer boundary along the unique outward normal ray based at c.

3.2 Radial Parametrization

The thickness function defines the radial map

$$\Phi : \partial C \longrightarrow \partial\Omega \setminus C, \qquad \Phi(c) = c + d(c)\nu(c). \tag{12}$$

By Proposition 2.3, Φ is bijective and its inverse is the restriction of the metric projection onto the convex core:

$$\Phi^{-1} = P_C\big|_{\partial\Omega\setminus C}. \tag{13}$$

Consequently, the outer boundary admits the global normal representation

$$\partial\Omega \setminus C = \{c + d(c)\nu(c) : c \in \partial C\}. \tag{14}$$

Equivalently, for every $x \in \partial\Omega \setminus C$,

$$x = \Phi(P_C(x)) = P_C(x) + d(P_C(x))\,\nu(P_C(x)). \tag{15}$$

The identities

$$P_C \circ \Phi = \mathrm{Id}_{\partial C}, \qquad \Phi \circ P_C = \mathrm{Id}_{\partial\Omega\setminus C} \tag{16}$$

will be used repeatedly below.

3.3 Regularity of the Thickness Function

We record here only the regularity needed to formulate the differential geometry of the radial map. Higher-order regularity is considered separately in Section 9.

Proposition 3.1. *Let $\Omega \in \mathcal{O}_C$. Then the thickness function*

$$d : \partial C \longrightarrow (0, \infty)$$

is locally Lipschitz.

Proof. Fix $c_0 \in \partial C$ and set

$$x_0 = \Phi(c_0) \in \partial\Omega \setminus C.$$

Since $\partial\Omega \setminus C$ is of class $C^{1,1}$, it admits in a neighbourhood of x_0 a $C^{1,1}$ defining function ρ, with

$$\partial\Omega = \{\rho = 0\}, \qquad \nabla\rho(x_0) \neq 0.$$

Choose a local $C^{1,1}$ parametrization $c = c(y)$ of ∂C near c_0 and consider

$$G(y,t) = \rho\big(c(y) + t\nu(c(y))\big).$$

The map G is locally Lipschitz in y. By the transversality condition (5), the derivative in the radial variable does not vanish at the intersection:

$$\partial_t G(y_0, d(c_0)) = \langle \nabla\rho(x_0), \nu(c_0)\rangle \neq 0.$$

After restricting the neighbourhood if necessary, this derivative is bounded away from zero. Thus there exists $\eta > 0$ such that

$$|\partial_t G(y,t)| \geq \eta$$

throughout a sufficiently small neighbourhood of $(y_0, d(c_0))$. Moreover, G is uniformly Lipschitz in the y-variable there; let L be a corresponding Lipschitz constant. Hence, for nearby y_1, y_2,

$$\eta\,|d(c(y_1)) - d(c(y_2))| \leq L|y_1 - y_2|.$$

Therefore d is locally Lipschitz. □

At points where d and the normal field ν are differentiable, the differential of the radial parametrization (12) is obtained directly from the product rule. For $v \in T_c\partial C$,

$$D\Phi(c)[v] = v + \langle \nabla_{\partial C} d(c), v\rangle\,\nu(c) + d(c)D\nu(c)[v]. \tag{17}$$

Using the convention

$$S_c = -D\nu(c)\big|_{T_c\partial C},$$

this becomes

$$D\Phi(c)[v] = \big(I - d(c)S_c\big)v + \langle \nabla_{\partial C} d(c), v\rangle\,\nu(c). \tag{18}$$

It is convenient to introduce the tangential operator

$$L_c := I - d(c)S_c. \tag{19}$$

At almost every $c \in \partial C$, its eigenvalues are

$$1 + d(c)\kappa_i(c), \qquad i = 1, \ldots, N-1,$$

and are therefore strictly positive. In particular, L_c is invertible almost everywhere.

The differential formula (18) will be the starting point for the computation of the normal to $\partial\Omega$ in Section 6.

4 Reciprocal Map and Geometric Round-Trip

4.1 Normal Rays from $\partial\Omega$

Let $\Omega \in \mathcal{O}_C$ and let $x \in \partial\Omega \setminus C$. Since $\partial\Omega \setminus C$ is an orientable $C^{1,1}$ hypersurface, its inward unit normal $n(x)$ is well defined. We consider the inward normal half-line

$$\Gamma_x = \{x + t\, n(x) : t \geq 0\}. \tag{20}$$

By the C-geometric normal property,

$$\Gamma_x \cap C \neq \varnothing.$$

Since C is compact and convex, the set of parameters

$$I_x = \{t \geq 0 : x + t\, n(x) \in C\}$$

is a nonempty compact interval. Moreover, $x \notin C$, so that

$$\inf I_x > 0.$$

We therefore define the first hitting time

$$t(x) = \min\{t > 0 : x + t\, n(x) \in C\}. \tag{21}$$

The corresponding point

$$x + t(x)n(x) \tag{22}$$

belongs to ∂C.

Thus every inward normal ray issued from $\partial\Omega \setminus C$ possesses a unique first intersection with the convex core.

4.2 Reciprocal Map

The first intersection of the inward normal ray with the convex core defines the reciprocal map

$$\pi : \partial\Omega \setminus C \longrightarrow \partial C, \qquad \pi(x) = x + t(x)n(x), \tag{23}$$

where $t(x) > 0$ is the first hitting time introduced in (21).

Equivalently,

$$t(x) = |\pi(x) - x|. \tag{24}$$

The reciprocal map should be distinguished from the metric projection onto C. In general,

$$\pi(x) \neq P_C(x), \tag{25}$$

since $\pi(x)$ is determined by the inward normal to $\partial\Omega$ at x, whereas $P_C(x)$ is determined by the outward normal geometry of the convex core.

Equality holds precisely when the inward normal ray at x passes through the metric projection $P_C(x)$.

4.3 Basic Properties

The reciprocal map is well defined on the whole outer boundary by the C-geometric normal property. Its regularity, however, depends on the manner in which the inward normal ray meets ∂C.

Definition 4.1. A point $x \in \partial\Omega \setminus C$ is called *return-transverse* if

$$\langle n(x), \nu(\pi(x))\rangle \neq 0. \tag{26}$$

Since $\pi(x)$ is the first point at which the inward ray meets the convex core, a transverse intersection satisfies in fact

$$\langle n(x), \nu(\pi(x))\rangle < 0.$$

Proposition 4.2. *Let $\Omega \in \mathcal{O}_C$.*

1. *The reciprocal map*
$$\pi : \partial\Omega \setminus C \longrightarrow \partial C$$
and the first hitting time t are well defined.
2. *Let $x_0 \in \partial\Omega \setminus C$ be return-transverse. Then t and π are locally Lipschitz in a neighbourhood of x_0.*
3. *If the boundaries are smoother near x_0 and $\pi(x_0)$, the corresponding local regularity of t and π follows from the implicit-function theorem, subject to the same transversality condition.*

Proof. The first assertion follows from Section 4.1.

For the local regularity, set

$$y_0 = \pi(x_0), \qquad t_0 = t(x_0).$$

Choose a $C^{1,1}$ defining function ρ_C for ∂C in a neighbourhood of y_0, normalized so that

$$\nabla\rho_C(y_0) = \nu(y_0).$$

Consider

$$H(x,t) = \rho_C\big(x + t\, n(x)\big), \tag{27}$$

for x on $\partial\Omega$ near x_0. At (x_0, t_0),

$$H(x_0, t_0) = 0,$$

and

$$\partial_t H(x_0, t_0) = \langle \nu(y_0), n(x_0)\rangle \neq 0. \tag{28}$$

Since ∂C and $\partial\Omega \setminus C$ are $C^{1,1}$, the normal field n and the local defining function ρ_C are Lipschitz. After restricting to a sufficiently small neighbourhood, the derivative in (28) remains bounded away from zero. Thus there exists $\eta > 0$ such that

$$|\partial_t H(x,t)| \geq \eta$$

in a sufficiently small neighbourhood of (x_0, t_0). It remains to see that $(x, t(x))$ stays in this neighbourhood for x near x_0, i.e. that t is continuous at x_0. Let $x_j \to x_0$ and let t' be a limit point of $t(x_j)$. Since C is closed, $x_0 + t'n(x_0) \in C$; as $x_0 \notin C$, $t' > 0$, so $t' \geq t_0$ by minimality of t_0. Conversely, C is convex with C^1 boundary and $\langle n(x_0), \nu(y_0)\rangle < 0$, so $x_0 + (t_0+\varepsilon)n(x_0) \in \operatorname{int}(C)$ for all small $\varepsilon > 0$; by continuity of n, also $x_j + (t_0+\varepsilon)n(x_j) \in \operatorname{int}(C)$ for large j, whence $t(x_j) \leq t_0 + \varepsilon$. Thus $t(x_j) \to t_0$. Since H is uniformly Lipschitz in the x-variable there, with some Lipschitz constant L, the identities

$$H(x_i, t(x_i)) = 0, \qquad i = 1, 2,$$

give

$$\eta\,|t(x_1) - t(x_2)| \leq L|x_1 - x_2|.$$

Hence t is locally Lipschitz. Since

$$\pi(x) = x + t(x)n(x)$$

and n is locally Lipschitz, π is locally Lipschitz as well.

The final assertion follows from the classical implicit-function theorem under the corresponding higher regularity assumptions. □

4.4 The Round-Trip

The radial and reciprocal maps combine to produce a geometric round-trip between the two boundaries,

$$\partial C \xrightarrow{\Phi} \partial\Omega \setminus C \xrightarrow{\pi} \partial C. \tag{29}$$

We define the associated return map by

$$F := \pi \circ \Phi : \partial C \longrightarrow \partial C, \qquad F(c) = \pi(\Phi(c)). \tag{30}$$

For $c \in \partial C$, set

$$x = \Phi(c), \qquad c' = F(c) = \pi(x).$$

The two legs of the construction are then

$$x = c + d(c)\nu(c), \qquad c' = x + t(x)n(x). \tag{31}$$

The outward radial structure is illustrated in Figure 1, while the inward return mechanism and the induced return map are shown in Figure 2.

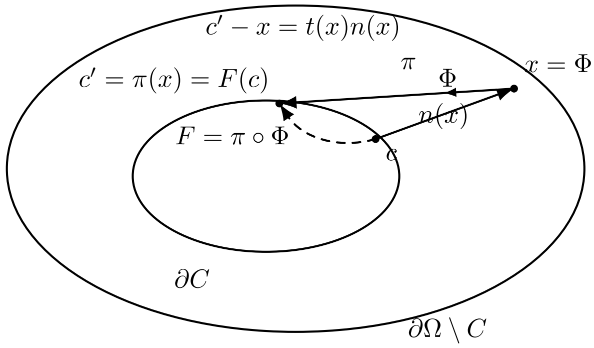

Figure 2. Reciprocal map and return map. Starting from $x = \Phi(c) \in \partial\Omega \setminus C$, the reciprocal map follows the inward normal $n(x)$ to its first intersection $c' = \pi(x) \in \partial C$. The induced return map on the convex core is $F = \pi \circ \Phi$. The sketch is schematic.

Figure 1 emphasizes the role of the metric projection, whereas Figure 2 highlights the distinction between the reciprocal map and the return map. By (13),

$$P_C(\Phi(c)) = c, \tag{32}$$

whereas in general

$$\pi(\Phi(c)) = F(c) \neq c. \tag{33}$$

Thus the outward and inward legs are governed by different normal geometries: the first by the convex core ∂C, the second by the outer boundary $\partial\Omega$.

The discrepancy between these two normal directions is the source of the nontrivial return dynamics studied below.

5 The Return Map and Discrete Dynamics

The geometric construction of Section 4 defines a self-map

$$F = \pi \circ \Phi : \partial C \longrightarrow \partial C.$$

We now study the discrete dynamics generated by successive applications of F. Throughout this section, all identities are exact unless an approximation is explicitly stated.

5.1 Discrete Iteration and Notation

Let $c_0 \in \partial C$. The return dynamics is defined recursively by

$$c_{k+1} = F(c_k), \qquad k \geq 0. \tag{34}$$

For each iterate c_k, we introduce the associated point on the outer boundary

$$x_k := \Phi(c_k) = c_k + d(c_k)\nu(c_k). \tag{35}$$

For brevity, we write

$$d_k := d(c_k),\ t_k := t(x_k),\ \nu_k := \nu(c_k),\ n_k := n(x_k). \tag{36}$$

Since

$$c_{k+1} = \pi(x_k),$$

the k-th step of the dynamics consists of the geometric excursion

$$c_k \xrightarrow{\Phi} x_k \xrightarrow{\pi} c_{k+1}. \tag{37}$$

The next subsection derives the exact displacement associated with one such step.

5.2 Fundamental Geometric Identity

The two legs of the k-th excursion give an exact relation between successive points of the return dynamics.

Proposition 5.1 (Exact displacement identity)**.** *For every $k \geq 0$,*

$$c_{k+1} - c_k = d_k\nu_k + t_kn_k. \tag{38}$$

Proof. By definition of the radial map,

$$x_k = c_k + d_k\nu_k.$$

By definition of the reciprocal map,

$$c_{k+1} = x_k + t_kn_k.$$

Substituting the first identity into the second gives

$$c_{k+1} = c_k + d_k\nu_k + t_kn_k,$$

which is equivalent to (38). □

Equation (38) is the basic closure relation for one step of the return dynamics. It contains no approximation and separates the outward radial displacement $d_k\nu_k$ from the inward normal displacement t_kn_k.

Taking scalar products with ν_k and n_k gives the exact relations

$$\langle c_{k+1} - c_k, \nu_k\rangle = d_k + t_k \langle n_k, \nu_k\rangle\,, \tag{39}$$

and

$$\langle c_{k+1} - c_k, n_k\rangle = d_k \langle \nu_k, n_k\rangle + t_k. \tag{40}$$

These identities will be used below when estimating the return distance and the displacement. In particular, neither (39) nor (40) determines t_k from d_k and the angle between the normals alone, because the displacement $c_{k+1} - c_k$ is itself nonzero in general.

5.3 Return Distance and Exact Closure Condition

The return distance t_k is determined by the condition that the inward normal ray from x_k meets the convex core for the first time at c_{k+1}. Thus

$$c_{k+1} = c_k + d_k\nu_k + t_kn_k \in \partial C, \tag{41}$$

with

$$t_k = \min\{t > 0 : c_k + d_k\nu_k + tn_k \in C\}\,. \tag{42}$$

Equivalently, if ρ_C is a local defining function for ∂C near c_{k+1}, chosen so that

$$\rho_C = 0 \quad \text{on } \partial C,$$

then t_k satisfies the exact implicit equation

$$\rho_C(c_k + d_k\nu_k + t_kn_k) = 0. \tag{43}$$

The following identity records the relation between the return distance and the displacement along ∂C.

Proposition 5.2 (Exact return-distance identity)**.** *For every $k \geq 0$,*

$$t_k = \frac{d_k - \langle c_{k+1} - c_k, \nu_k\rangle}{-\langle n_k, \nu_k\rangle}. \tag{44}$$

Here

$$-\langle n_k, \nu_k\rangle > 0$$

by the orientation and radial transversality of the intersection $x_k = \Phi(c_k)$.

Proof. Taking the scalar product of the exact displacement identity (38) with ν_k gives

$$\langle c_{k+1} - c_k, \nu_k\rangle = d_k + t_k \langle n_k, \nu_k\rangle\,.$$

Solving for t_k yields (44). □

Since ν_k is the outward normal to the supporting hyperplane of the convex set C at c_k, and since $c_{k+1} \in C$, one has

$$\langle c_{k+1} - c_k, \nu_k\rangle \leq 0. \tag{45}$$

Consequently,

$$t_k \geq \frac{d_k}{-\langle n_k, \nu_k\rangle} = \frac{d_k}{|\langle n_k, \nu_k\rangle|}. \tag{46}$$

In particular, the return distance is not determined by d_k and the angle between n_k and ν_k alone. The additional term

$$\langle c_{k+1} - c_k, \nu_k\rangle$$

measures the normal component, relative to the supporting hyperplane at c_k, of the displacement of the return point on ∂C.

At a fixed point, where $c_{k+1} = c_k$, the correction term vanishes and (44) reduces to

$$t_k = \frac{d_k}{|\langle n_k, \nu_k \rangle|}.$$

As will be shown later, at such a point $n_k = -\nu_k$, and therefore $t_k = d_k$.

6 First-Order Expansion of the Return Map

We now derive the local expansion of the return map from the exact geometry of the radial parametrization. The derivation is organized so that exact identities are separated from asymptotic statements. Throughout this section, all differential identities are understood at points where the relevant derivatives exist. Under the $C^{1,1}$ and Lipschitz assumptions introduced above, this holds almost everywhere on ∂C.

6.1 Exact Normal to the Outer Boundary

Let $c \in \partial C$ be a point at which d and ν are differentiable, and set

$$x = \Phi(c), \qquad g_c := \nabla_{\partial C} d(c).$$

Recall from (19) that

$$L_c = I - d(c) S_c.$$

Since the eigenvalues of L_c are

$$1 + d(c)\kappa_i(c) > 0,$$

the operator $L_c : T_c\partial C \to T_c\partial C$ is invertible.

Define the tangent vector

$$w_c := L_c^{-1} g_c = \big(I - d(c)S_c\big)^{-1} \nabla_{\partial C} d(c). \tag{47}$$

Proposition 6.1 (Exact normal formula). *At $x = \Phi(c)$, the outward unit normal to $\partial\Omega$ is*

$$N_\Omega(x) = \frac{\nu(c) - w_c}{\sqrt{1 + |w_c|^2}}, \tag{48}$$

and therefore the inward unit normal is

$$n(x) = \frac{-\nu(c) + w_c}{\sqrt{1 + |w_c|^2}}. \tag{49}$$

Proof. By (18), for every $v \in T_c\partial C$,

$$D\Phi(c)[v] = L_c v + \langle g_c, v \rangle \nu(c).$$

Since the shape operator S_c is self-adjoint on $T_c\partial C$, the operator

$$L_c = I - d(c)S_c$$

is self-adjoint as well. Hence, using $L_c w_c = g_c$,

$$\begin{aligned} \langle \nu(c) - w_c, D\Phi(c)[v] \rangle &= -\langle w_c, L_c v \rangle + \langle g_c, v \rangle \\ &= -\langle L_c w_c, v \rangle + \langle g_c, v \rangle \\ &= 0. \end{aligned}$$

Hence $\nu(c) - w_c$ is normal to the image hypersurface $\partial\Omega$ at $x = \Phi(c)$.

Moreover, since $w_c \in T_c\partial C$,

$$|\nu(c) - w_c|^2 = 1 + |w_c|^2.$$

Thus normalization gives (48).

Finally,

$$\langle N_\Omega(x), \nu(c) \rangle = \frac{1}{\sqrt{1 + |w_c|^2}} > 0,$$

so this choice has the outward orientation. Its negative is the inward unit normal, which gives (49). □

Remark 6.2. If $\nabla_{\partial C} d(c) = 0$, then $w_c = 0$ and hence

$$N_\Omega(\Phi(c)) = \nu(c), \qquad n(\Phi(c)) = -\nu(c).$$

6.2 Exact Decomposition and Closure Equation

The exact normal formula reduces the return geometry to a scalar closure problem. Let $c \in \partial C$ be a point at which the quantities introduced in Section 6.1 are defined, and set

$$x = \Phi(c), \qquad t_c := t(\Phi(c)).$$

For brevity, write

$$d = d(c), \qquad \nu = \nu(c), \qquad w = w_c.$$

We introduce the scaled return parameter

$$\sigma(c) := \frac{t_c}{\sqrt{1 + |w_c|^2}}. \tag{50}$$

Proposition 6.3 (Exact decomposition of the return displacement). *The return displacement satisfies*

$$F(c) - c = \sigma(c) w_c + \big(d(c) - \sigma(c)\big)\nu(c). \tag{51}$$

In particular, with $P_{T_c\partial C}$ denoting the orthogonal projection of $\mathbb{R}^N$ onto $T_c\partial C$,

$$P_{T_c\partial C}\big(F(c) - c\big) = \sigma(c) w_c, \tag{52}$$

$$\langle F(c) - c, \nu(c) \rangle = d(c) - \sigma(c). \tag{53}$$

Proof. By the exact displacement identity (38),

$$F(c) - c = d(c)\nu(c) + t_c\, n(\Phi(c)).$$

Using (49),

$$t_c\, n(\Phi(c)) = \frac{t_c}{\sqrt{1+|w_c|^2}}\big(-\nu(c) + w_c\big).$$

The definition (50) therefore gives

$$F(c) - c = d(c)\nu(c) + \sigma(c)\big(-\nu(c) + w_c\big),$$

which is precisely (51). Since $w_c \in T_c\partial C$ and $\nu(c) \perp T_c\partial C$, the two component identities follow. □

Lemma 6.4 (Local return near a critical point). *Let $c_* \in \partial C$ be a point at which d is differentiable and*

$$\nabla_{\partial C} d(c_*) = 0.$$

Then

$$F(c_*) = c_*. \tag{54}$$

Moreover, the inward normal ray from $x_* = \Phi(c_*)$ meets ∂C transversely at c_*. Consequently, F is continuous at c_*: for every neighbourhood $U \subset \partial C$ of c_* contained in a single local coordinate chart of ∂C there is a neighbourhood $V \subset \partial C$ of c_* such that

$$F(V) \subset U.$$

Proof. Since

$$\nabla_{\partial C} d(c_*) = 0,$$

equation (47) gives $w_{c_*} = 0$. Hence the exact normal formula (49) yields

$$n(\Phi(c_*)) = -\nu(c_*).$$

Therefore the inward normal ray issued from

$$\Phi(c_*) = c_* + d(c_*)\nu(c_*)$$

is the radial segment directed toward c_*. Its first intersection with the convex core is c_*, and consequently

$$F(c_*) = c_*.$$

Furthermore,

$$\langle n(\Phi(c_*)), \nu(c_*)\rangle = -1,$$

so the intersection is transverse. Proposition 4.2 therefore gives local continuity of the reciprocal map near $\Phi(c_*)$. Since the radial map Φ is locally continuous, the return map $F = \pi \circ \Phi$ is continuous near c_*. The final assertion is precisely the continuity of F at c_*: given a coordinate neighbourhood U of c_*, choose V so that $F(V) \subset U$. □

We now restrict to the local-return regime provided by Lemma 6.4. Let c_* be the critical point appearing there. After shrinking the neighbourhood V of c_* if necessary, the $C^{1,1}$ regularity of ∂C provides a radius $r > 0$ such that, for every $c \in V$, the portion of ∂C near c can be represented as a normal graph

$$u \longmapsto c + u + h_c(u)\nu(c), \qquad u \in U_c \subset T_c\partial C, \tag{55}$$

where U_c contains the tangent ball of radius r and

$$h_c(0) = 0, \qquad Dh_c(0) = 0. \tag{56}$$

Moreover, after possibly shrinking V once more, the $C^{1,1}$ bounds may be chosen uniformly:

$$|h_c(u)| \le K|u|^2, \qquad c \in V, \quad u \in U_c, \tag{57}$$

for some constant $K > 0$.

Since $F(c_*) = c_*$ and F is continuous near c_* by Lemma 6.4, one has

$$|F(c) - c| \longrightarrow 0 \qquad \text{as } c \longrightarrow c_*.$$

Hence, after shrinking V again if necessary, $F(c)$ belongs to the above normal-graph neighbourhood based at c for every $c \in V$.

At every such c at which d and ν are differentiable, there is therefore a unique $u_c \in U_c$ such that

$$F(c) - c = u_c + h_c(u_c)\nu(c). \tag{58}$$

On the other hand, the exact return decomposition (51) gives

$$F(c) - c = \sigma(c) w_c + \big(d(c) - \sigma(c)\big)\nu(c).$$

Taking the orthogonal projection onto $T_c\partial C$ and the scalar product with $\nu(c)$ yields

$$u_c = \sigma(c) w_c$$

and

$$h_c(u_c) = d(c) - \sigma(c).$$

Consequently,

$$d(c) - \sigma(c) = h_c\big(\sigma(c) w_c\big). \tag{59}$$

Equation (59) immediately implies

$$|d(c) - \sigma(c)| \le K\, \sigma(c)^2 |w_c|^2. \tag{60}$$

Thus the normal component of the return displacement is of second order in the slope w_c.

For a convex core, the local graph lies on the inward side of its supporting tangent hyperplane, and hence

$$h_c(u) \le 0$$

for u sufficiently small. Consequently,

$$\sigma(c) \ge d(c). \tag{61}$$

Using (50), this gives

$$t_c \ge d(c)\sqrt{1+|w_c|^2}. \tag{62}$$

Remark 6.5. If $w_c = 0$, then (59) gives $\sigma(c) = d(c)$. Hence

$$t_c = d(c), \qquad F(c) = c.$$

Thus vanishing tangential slope produces an exact fixed point, not merely an approximate one.

6.3 First-Order Expansion

We can now derive the first-order expansion of the return map. The expansion is naturally expressed in terms of the tangential slope

$$w_c = \big(I - d(c)S_c\big)^{-1}\nabla_{\partial C} d(c).$$

Theorem 6.6 (Quadratic remainder estimate for the return map). *Let $c_* \in \partial C$ be a critical point as in Lemma 6.4, and let V be a sufficiently small local-return neighbourhood of c_*. Then there exists a constant $\Lambda > 0$ such that, at every $c \in V$ where d and ν are differentiable,*

$$F(c) - c = d(c)w_c + R(c), \tag{63}$$

where

$$|R(c)| \le \Lambda |w_c|^2. \tag{64}$$

Equivalently,

$$F(c) - c = d(c)\big(I - d(c)S_c\big)^{-1}\nabla_{\partial C} d(c) + R(c), \tag{65}$$

with

$$|R(c)| \le \Lambda \left|\nabla_{\partial C} d(c)\right|^2. \tag{66}$$

Thus, at every differentiability point in the above neighbourhood, the return displacement satisfies the quadratic remainder estimate

$$F(c)-c = d(c)\big(I-d(c)S_c\big)^{-1}\nabla_{\partial C} d(c)+O\big(|\nabla_{\partial C} d(c)|^2\big). \tag{67}$$

Proof. By Proposition 6.3,

$$F(c) - c = \sigma(c)w_c + \big(d(c) - \sigma(c)\big)\nu(c). \tag{68}$$

The exact closure equation (59), together with the quadratic estimate for the local graph of ∂C, gives

$$|d(c) - \sigma(c)| \le K\,\sigma(c)^2 |w_c|^2. \tag{69}$$

By Lemma 6.4 and Proposition 4.2, the return distance $t(\Phi(c))$ is locally bounded in V. Since

$$\sigma(c) = \frac{t(\Phi(c))}{\sqrt{1+|w_c|^2}},$$

there exists $M > 0$ such that

$$0 < \sigma(c) \le M$$

throughout V. Hence

$$|d(c) - \sigma(c)| \le KM^2 |w_c|^2. \tag{70}$$

Subtracting $d(c)w_c$ from (68) yields

$$\begin{aligned} F(c) - c - d(c)w_c &= \big(\sigma(c) - d(c)\big)w_c + \big(d(c) - \sigma(c)\big)\nu(c) \\ &= \big(\sigma(c) - d(c)\big)\big(w_c - \nu(c)\big). \end{aligned}$$

Therefore

$$|F(c) - c - d(c)w_c| \le |d(c) - \sigma(c)|\sqrt{1+|w_c|^2}.$$

After shrinking V if necessary, w_c is bounded at the differentiability points under consideration. Combining this with (70) gives

$$|F(c) - c - d(c)w_c| \le \Lambda |w_c|^2,$$

which proves (63) and (64).

It remains to express the estimate in terms of the thickness gradient. Since the eigenvalues of

$$L_c = I - d(c)S_c$$

are

$$1 + d(c)\kappa_i(c) \ge 1,$$

one has

$$\|L_c^{-1}\| \le 1. \tag{71}$$

Consequently,

$$|w_c| = \left|L_c^{-1}\nabla_{\partial C} d(c)\right| \le \left|\nabla_{\partial C} d(c)\right|.$$

Substitution into the preceding estimate gives (66) and completes the proof. □

It is convenient to introduce the positive tangential operator

$$B_c := d(c)\big(I - d(c)S_c\big)^{-1}. \quad (72)$$

Its eigenvalues in the principal directions of ∂C are

$$\beta_i(c) = \frac{d(c)}{1 + d(c)\kappa_i(c)} > 0. \quad (73)$$

Hence the quadratic remainder estimate takes the compact form

$$F(c) - c = B_c \nabla_{\partial C} d(c) + O\big(|\nabla_{\partial C} d(c)|^2\big). \quad (74)$$

Remark 6.7. Under the $C^{1,1}$ assumptions used above, Theorem 6.6 is a quadratic remainder estimate at points where d and ν are differentiable, hence almost everywhere on ∂C.

If, in addition, d is of class C^1 in a neighbourhood of the critical point c_*, then

$$\nabla_{\partial C} d(c) \longrightarrow 0 \qquad \text{as } c \longrightarrow c_*.$$

In this case the estimate becomes a genuine local asymptotic expansion:

$$F(c) - c = B_c \nabla_{\partial C} d(c) + o(|\nabla_{\partial C} d(c)|),$$

along points where the shape operator is defined.

If ∂C is moreover of class C^2 near c_*, then S_c is defined continuously and the expansion holds in the classical pointwise sense.

6.4 Circle and Sphere Consistency Checks

The sign and curvature dependence in Theorem 6.6 can be checked explicitly when the convex core is a Euclidean sphere.

Spherical core

Let

$$C = \overline{B_R(0)} \subset \mathbb{R}^N, \qquad \partial C = R\mathbb{S}^{N-1}.$$

For the outward orientation,

$$\nu(c) = \frac{c}{R}, \qquad S_c = -\frac{1}{R}I$$

on $T_c\partial C$. Hence

$$L_c = I - d(c)S_c = \left(1 + \frac{d(c)}{R}\right)I, \quad (75)$$

and therefore

$$w_c = \frac{R}{R + d(c)}\nabla_{\partial C} d(c). \quad (76)$$

The first-order expansion (65) becomes

$$F(c) - c = \frac{d(c)R}{R + d(c)}\nabla_{\partial C} d(c) + O\big(|\nabla_{\partial C} d(c)|^2\big). \quad (77)$$

In particular, the leading displacement has the same direction as the tangential gradient of the thickness function.

The closure equation can also be checked directly. In normal coordinates based at c, the sphere is represented by

$$h_c(u) = -R + \sqrt{R^2 - |u|^2}. \quad (78)$$

Thus

$$h_c(u) = -\frac{|u|^2}{2R} + O(|u|^4). \quad (79)$$

Substitution into (59) gives

$$d(c) - \sigma(c) = -R + \sqrt{R^2 - \sigma(c)^2|w_c|^2}. \quad (80)$$

Equivalently,

$$\big(R + d(c) - \sigma(c)\big)^2 + \sigma(c)^2|w_c|^2 = R^2. \quad (81)$$

For $|w_c| \to 0$, the branch corresponding to the first intersection with the sphere satisfies

$$\sigma(c) = d(c) + O(|w_c|^2), \quad (82)$$

which is consistent with Theorem 6.6.

Unit circle

Consider now the planar case

$$C = \overline{B_1(0)} \subset \mathbb{R}^2.$$

Write

$$c(\theta) = (\cos\theta, \sin\theta),$$

and let e_θ denote the positively oriented unit tangent. Then

$$\nu(\theta) = c(\theta), \qquad S = -I,$$

and

$$\nabla_{\partial C} d(\theta) = d'(\theta)e_\theta.$$

Consequently,

$$w(\theta) = \frac{d'(\theta)}{1 + d(\theta)}e_\theta. \quad (83)$$

Introduce

$$p(\theta) := \frac{d'(\theta)}{1 + d(\theta)}. \quad (84)$$

The outer point is

$$x(\theta) = \big(1 + d(\theta)\big)\nu(\theta),$$

and the exact inward normal formula gives

$$n(x(\theta)) = \frac{-\nu(\theta) + p(\theta)e_\theta}{\sqrt{1 + p(\theta)^2}}. \tag{85}$$

Writing

$$\sigma = \frac{t}{\sqrt{1+p^2}},$$

the return point is therefore

$$F(c(\theta)) = (1 + d - \sigma)\nu(\theta) + \sigma p\, e_\theta. \tag{86}$$

Since $F(c(\theta))$ belongs to the unit circle, the exact closure condition is

$$(1 + d - \sigma)^2 + \sigma^2 p^2 = 1. \tag{87}$$

Solving the corresponding quadratic equation and choosing the branch giving the first intersection yields

$$\sigma = \frac{1 + d - \sqrt{1 - d(2+d)p^2}}{1 + p^2}. \tag{88}$$

Here $d = d(\theta)$ and $p = p(\theta)$. For $p \to 0$,

$$\sigma = d + O(p^2). \tag{89}$$

Let

$$F(c(\theta)) = c(\theta + \delta(\theta)).$$

Taking the tangential component of (86) gives

$$\sin\delta(\theta) = \sigma(\theta)p(\theta). \tag{90}$$

Using (89) and (84), we obtain

$$\delta(\theta) = \frac{d(\theta)}{1 + d(\theta)} d'(\theta) + O\big(|d'(\theta)|^2\big)\,. \tag{91}$$

Equivalently, in ambient coordinates,

$$F(c(\theta)) - c(\theta) = \frac{d(\theta)}{1 + d(\theta)} d'(\theta)e_\theta + O\big(|d'(\theta)|^2\big)\,. \tag{92}$$

Thus the unit-circle calculation reproduces exactly the leading term predicted by Theorem 6.6. In particular, its coefficient is positive and equals

$$\frac{d(\theta)}{1 + d(\theta)}.$$

The circle therefore provides a direct consistency check both for the sign and for the curvature factor in the return-map expansion.

6.5 Geometric Interpretation

The expansion (74) shows that, to first order, the return displacement is obtained by applying the positive tangential operator

$$B_c = d(c)\big(I - d(c)S_c\big)^{-1}$$

to the tangential gradient of the thickness function:

$$F(c) - c = B_c \nabla_{\partial C} d(c) + O\big(|\nabla_{\partial C} d(c)|^2\big)\,. \tag{93}$$

Thus the leading-order dynamics is not an ordinary gradient step, but a curvature-dependent preconditioned gradient step on ∂C.

In a principal direction $e_i(c)$ of the convex core,

$$S_c e_i(c) = -\kappa_i(c)e_i(c),$$

and hence

$$B_c e_i(c) = \frac{d(c)}{1 + d(c)\kappa_i(c)} e_i(c). \tag{94}$$

Therefore curvature modifies the strength of the return displacement anisotropically. Directions with larger principal curvature are weighted by the smaller factor

$$\frac{d(c)}{1 + d(c)\kappa_i(c)}.$$

Since every eigenvalue of B_c is positive,

$$\langle B_c \nabla_{\partial C} d(c), \nabla_{\partial C} d(c)\rangle \geq 0, \tag{95}$$

with strict inequality whenever $\nabla_{\partial C} d(c) \neq 0$. Hence the leading-order displacement points in a gradient-ascent direction for the thickness function, with the metric distorted by the curvature of the convex core.

This interpretation should be understood locally. The expansion does not by itself imply that

$$d(F(c)) > d(c)$$

for every noncritical point, since such a monotonicity statement also depends on the size of the step and on higher-order terms. Accordingly, no global Lyapunov conclusion is drawn at this stage.

At a critical point c_* of d,

$$\nabla_{\partial C} d(c_*) = 0,$$

the leading-order displacement vanishes. As shown in Lemma 6.4, this is in fact an exact statement:

$$\nabla_{\partial C} d(c_*) = 0 \quad\Longrightarrow\quad F(c_*) = c_*. \tag{96}$$

The converse and the local stability of such fixed points will be studied in the next section.

7 Fixed Points, Linearization, and Local Stability

We now derive the local dynamical consequences of the return-map expansion. The exact geometry established in Section 6 first identifies the fixed points of the return map. For the subsequent linearization and stability analysis, stronger local smoothness assumptions will be introduced explicitly when needed.

7.1 Fixed Points and Critical Points

The exact decomposition of the return displacement gives a direct characterization of the fixed points.

Theorem 7.1 (Fixed points and critical points). *Let $c \in \partial C$ be a point at which d and ν are differentiable. Then*

$$F(c) = c \quad \Longleftrightarrow \quad \nabla_{\partial C} d(c) = 0. \tag{97}$$

Proof. Suppose first that

$$\nabla_{\partial C} d(c) = 0.$$

By (47),

$$w_c = 0.$$

The exact inward-normal formula (49) therefore gives

$$n(\Phi(c)) = -\nu(c).$$

Hence the inward normal ray from

$$\Phi(c) = c + d(c)\nu(c)$$

runs back along the same normal line toward c. Since c is the metric projection of $\Phi(c)$ onto the convex set C, its first intersection with C is c. Consequently,

$$F(c) = c.$$

Conversely, suppose that

$$F(c) = c.$$

By the exact return decomposition (51),

$$0 = \sigma(c)w_c + \big(d(c) - \sigma(c)\big)\nu(c).$$

The first term is tangent to ∂C at c, whereas the second is normal to ∂C. Since these subspaces are orthogonal, both components must vanish:

$$\sigma(c)w_c = 0, \qquad d(c) - \sigma(c) = 0. \tag{98}$$

Because $t(\Phi(c)) > 0$, the definition

$$\sigma(c) = \frac{t(\Phi(c))}{\sqrt{1 + |w_c|^2}}$$

implies $\sigma(c) > 0$. Hence

$$w_c = 0.$$

Since

$$w_c = \big(I - d(c)S_c\big)^{-1}\nabla_{\partial C} d(c)$$

and $I - d(c)S_c$ is invertible, we conclude that

$$\nabla_{\partial C} d(c) = 0.$$

This proves (97). □

Remark 7.2. Under the $C^{1,1}$ framework of the preceding sections, Theorem 7.1 is an almost-everywhere statement, because d and the normal field are differentiable almost everywhere.

If d is C^1 and ∂C is C^2 in a neighbourhood of a point under consideration, the equivalence

$$F(c) = c \quad \Longleftrightarrow \quad \nabla_{\partial C} d(c) = 0$$

holds in the classical pointwise sense.

7.2 Linearization at a Critical Point

We now pass from the $C^{1,1}$ framework used for the first-order expansion to the classical differentiable setting required for a pointwise linearization. Throughout this subsection, assume that ∂C is of class C^2 and that the thickness function d is of class C^2 in a neighbourhood of a critical point $c_* \in \partial C$.

Set

$$d_* := d(c_*), \qquad S_* := S_{c_*},$$

and define

$$B_* := d_*\big(I - d_* S_*\big)^{-1}. \tag{99}$$

Since c_* is critical,

$$\nabla_{\partial C} d(c_*) = 0,$$

and Theorem 7.1 gives

$$F(c_*) = c_*.$$

To avoid ambiguity between the bilinear Hessian and its associated endomorphism, let

$$H_* : T_{c_*}\partial C \longrightarrow T_{c_*}\partial C$$

denote the self-adjoint operator determined by

$$\langle H_* v, z\rangle = \mathrm{Hess}_{\partial C}\, d(c_*)[v, z], \qquad v, z \in T_{c_*}\partial C. \tag{100}$$

Theorem 7.3 (Linearization at a critical point)**.** *Under the assumptions above, the derivative of the return map at c_* is*

$$DF(c_*)\big|_{T_{c_*}\partial C} = I + B_* H_*. \tag{101}$$

Equivalently,

$$DF(c_*)\big|_{T_{c_*}\partial C} = I + d_*\big(I - d_* S_*\big)^{-1} H_*. \tag{102}$$

Proof. Choose a local C^2 coordinate parametrization

$$c : U \subset T_{c_*}\partial C \longrightarrow \partial C$$

such that

$$c(0) = c_*, \qquad Dc(0) = I.$$

After shrinking U if necessary, we identify the nearby tangent spaces with $T_{c_*}\partial C$ through the corresponding local coordinate frame.

Since c is C^2,

$$c(u) = c_* + u + O(|u|^2) \qquad \text{as } u \to 0. \tag{103}$$

By Theorem 6.6,

$$F(c(u)) - c(u) = B_{c(u)} \nabla_{\partial C} d(c(u)) + R(c(u)), \tag{104}$$

where

$$B_c = d(c)\big(I - d(c)S_c\big)^{-1}$$

and

$$|R(c)| \le \Lambda |\nabla_{\partial C} d(c)|^2. \tag{105}$$

Because ∂C and d are of class C^2, the map $c \mapsto B_c$ is continuous near c_*. Hence

$$B_{c(u)} = B_* + o(1). \tag{106}$$

Moreover,

$$\nabla_{\partial C} d(c_*) = 0.$$

At a critical point, the differential of the tangential gradient is the Hessian operator H_*. Therefore, in the above local trivialization,

$$\nabla_{\partial C} d(c(u)) = H_* u + o(|u|). \tag{107}$$

In particular,

$$|\nabla_{\partial C} d(c(u))| = O(|u|).$$

It follows from (105) that

$$R(c(u)) = O(|u|^2) = o(|u|). \tag{108}$$

Combining (106) and (107), we obtain

$$B_{c(u)} \nabla_{\partial C} d(c(u)) = B_* H_* u + o(|u|). \tag{109}$$

Substituting (108) and (109) into (104) gives

$$F(c(u)) - c(u) = B_* H_* u + o(|u|).$$

Using (103),

$$F(c(u)) = c_* + \big(I + B_* H_*\big)u + o(|u|).$$

Hence the local representation of F is Fréchet differentiable at $u = 0$, and

$$DF(c_*)\big|_{T_{c_*}\partial C} = I + B_* H_*.$$

This proves (101). □

Remark 7.4. Although Theorem 7.3 is derived from the local expansion of Section 6, formula (101) is the exact derivative of the return map at the fixed point. No remainder term remains in the linearization.

7.3 Spectral Form of the Linearization

The linearization obtained in Theorem 7.3 involves the product $B_* H_*$ of two self-adjoint operators. Although this product is not self-adjoint in general, its spectrum has a simple symmetric representation because B_* is positive definite.

Recall that

$$B_* = d_*\big(I - d_* S_*\big)^{-1}.$$

Since $d_* > 0$ and the eigenvalues of $I - d_* S_*$ are $1 + d_* \kappa_i > 0$, the operator B_* is positive definite and admits a unique positive square root $B_*^{1/2}$.

Define

$$K_* := B_*^{1/2} H_* B_*^{1/2}. \tag{110}$$

Proposition 7.5 (Symmetric spectral representation)**.** *The operator K_* is self-adjoint, and $B_* H_*$ is similar to K_*. More precisely,*

$$B_* H_* = B_*^{1/2} K_* B_*^{-1/2}. \tag{111}$$

Consequently, $B_* H_*$ is diagonalizable over $\mathbb{R}$ and all of its eigenvalues are real.

Proof. Since both $B_*^{1/2}$ and H_* are self-adjoint,

$$K_*^* = B_*^{1/2} H_* B_*^{1/2} = K_*.$$

Thus K_* is self-adjoint.

Moreover,

$$\begin{aligned} B_*^{1/2} K_* B_*^{-1/2} &= B_*^{1/2} \big(B_*^{1/2} H_* B_*^{1/2} \big) B_*^{-1/2} \\ &= B_* H_*, \end{aligned}$$

which proves (111). Since a self-adjoint operator has a real spectrum and is diagonalizable, the same is true for the similar operator $B_* H_*$. □

Let

$$\mu_1, \ldots, \mu_{N-1}$$

denote the eigenvalues of $B_* H_*$, counted with multiplicity. Equivalently, they are the eigenvalues of the self-adjoint operator K_*. By (101), the eigenvalues of the derivative of the return map are therefore

$$\lambda_j = 1 + \mu_j, \qquad j = 1, \ldots, N-1. \tag{112}$$

Proposition 7.6 (Inertia of the preconditioned Hessian)**.** *The operators K_* and H_* have the same numbers of positive, negative, and zero eigenvalues. Consequently, the signs of the eigenvalues μ_j are determined by the Morse type of the critical point c_*.*

Proof. For every $v \in T_{c_*} \partial C$,

$$\langle K_* v, v \rangle = \left\langle H_* B_*^{1/2} v, B_*^{1/2} v \right\rangle .$$

Since $B_*^{1/2}$ is invertible, the quadratic forms associated with K_* and H_* are related by an invertible change of variables. Sylvester's law of inertia therefore implies that they have the same inertia. □

In particular:

- if c_* is a strict local minimum and H_* is positive definite, then

$$\mu_j > 0 \qquad \text{for all } j;$$

- if c_* is a strict local maximum and H_* is negative definite, then

$$\mu_j < 0 \qquad \text{for all } j;$$

- if c_* is a nondegenerate saddle point, then the set of eigenvalues $\{\mu_j\}$ contains both positive and negative values.

The fixed point c_* is linearly attracting precisely when

$$|\lambda_j| < 1 \qquad \text{for every } j, \tag{113}$$

or equivalently,

$$-2 < \mu_j < 0 \qquad \text{for every } j. \tag{114}$$

Thus negative definiteness of the Hessian is necessary for linear attraction at a nondegenerate critical point, but it is not by itself sufficient: the negative eigenvalues of the preconditioned Hessian must also remain above the threshold -2.

7.4 Local Stability of Nondegenerate Critical Points

We now translate the spectral information obtained above into a local stability classification of nondegenerate fixed points.

Theorem 7.7 (Local stability classification)**.** *Let $c_* \in \partial C$ be a nondegenerate critical point of d. Assume that ∂C and d are of class C^2 in a neighbourhood of c_*. Let*

$$\mu_1, \ldots, \mu_{N-1}$$

be the eigenvalues of the preconditioned Hessian

$$B_* H_*, \qquad B_* = d_* \big(I - d_* S_* \big)^{-1}.$$

Then the eigenvalues of the linearized return map are

$$\lambda_j = 1 + \mu_j.$$

The following alternatives hold.

1. *If c_* is a strict local minimum of d, then*

$$\mu_j > 0 \qquad \text{for all } j,$$

and hence

$$\lambda_j > 1 \qquad \text{for all } j.$$

Therefore c_* is a hyperbolic repelling fixed point.

2. *If c_* is a strict local maximum of d, then*

$$\mu_j < 0 \qquad \text{for all } j.$$

The fixed point is linearly hyperbolic attracting if and only if

$$-2 < \mu_j < 0 \qquad \text{for all } j. \tag{115}$$

Equivalently,

$$|\lambda_j| < 1 \qquad \text{for all } j.$$

3. *If c_* is a nondegenerate saddle point of d, then some μ_j are positive and some are negative. In particular, at least one eigenvalue of $DF(c_*)$ satisfies*

$$\lambda_j > 1.$$

Hence c_* is unstable.

Proof. The spectral relation

$$\lambda_j = 1 + \mu_j$$

follows from (112).

If c_* is a strict local minimum, the Hessian H_* is positive definite. Proposition 7.6 therefore gives $\mu_j > 0$ for every j, and hence $\lambda_j > 1$. Thus the fixed point is repelling.

If c_* is a strict local maximum, H_* is negative definite, so $\mu_j < 0$ for every j. Linear attraction is equivalent to

$$|1 + \mu_j| < 1$$

for every j, which is precisely

$$-2 < \mu_j < 0.$$

Finally, if c_* is a nondegenerate saddle point, then H_* has both positive and negative eigenvalues. By Proposition 7.6, the same is true of the set $\{\mu_j\}$. Hence at least one μ_j is positive, so the corresponding eigenvalue

$$\lambda_j = 1 + \mu_j$$

satisfies $\lambda_j > 1$. Therefore the fixed point is unstable. □

Remark 7.8. A strict local maximum is not automatically attracting. The negative eigenvalues of the preconditioned Hessian must satisfy the quantitative bound

$$\mu_j > -2.$$

If some $\mu_j = -2$, then the corresponding multiplier equals -1 and the linearization is nonhyperbolic. If some $\mu_j < -2$, then the corresponding multiplier satisfies

$$\lambda_j < -1,$$

and the fixed point is unstable in that direction.

Corollary 7.9. *Under the assumptions of Theorem 7.7, nondegenerate local minima of the thickness function are repelling fixed points of the return map. Nondegenerate local maxima are the only critical points that can be locally attracting, subject to the spectral condition* (115).

8 Numerical Validation

The purpose of this section is to provide direct numerical checks of the return-map formulas derived in Sections 6 and 7. We restrict the computations to the unit-circle core, for which the return step can be evaluated explicitly. This allows the numerical iteration to be performed from the exact geometric equations rather than from the first-order approximation.

The examples below are intended only to validate the first-order displacement and the local multiplier at a fixed point. No global convergence or Lyapunov conclusion is inferred from these computations.

8.1 Exact Numerical Return Map on the Unit Circle

Let

$$C = \overline{B_1(0)} \subset \mathbb{R}^2, \qquad c(\theta) = (\cos\theta, \sin\theta),$$

and let $d(\theta) > 0$ be a smooth 2π-periodic thickness function. Denote by

$$e_\theta = (-\sin\theta, \cos\theta)$$

the positively oriented unit tangent.

As derived in Section 6.4, define

$$p(\theta) = \frac{d'(\theta)}{1 + d(\theta)}. \tag{116}$$

The exact inward normal at the corresponding point of the outer boundary is

$$n(\Phi(c(\theta))) = \frac{-c(\theta) + p(\theta)e_\theta}{\sqrt{1 + p(\theta)^2}}. \tag{117}$$

Introducing

$$\sigma = \frac{t}{\sqrt{1 + p^2}},$$

the condition that the return point belongs to the unit circle gives the exact closure equation

$$(1 + d - \sigma)^2 + \sigma^2 p^2 = 1. \tag{118}$$

The branch corresponding to the first intersection of the inward normal ray with the convex core is

$$\sigma(\theta) = \frac{1 + d(\theta) - \sqrt{1 - d(\theta)\big(2 + d(\theta)\big)p(\theta)^2}}{1 + p(\theta)^2}. \tag{119}$$

For numerical purposes, set

$$a(\theta) = 1 + d(\theta) - \sigma(\theta), \qquad b(\theta) = \sigma(\theta)p(\theta). \tag{120}$$

Then

$$F(c(\theta)) = a(\theta)c(\theta) + b(\theta)e_\theta. \tag{121}$$

The closure equation implies

$$a(\theta)^2 + b(\theta)^2 = 1.$$

Consequently, the exact angular displacement is obtained from

$$\delta(\theta) = \operatorname{atan2}\big(b(\theta), a(\theta)\big). \tag{122}$$

and one iteration of the return map is

$$\theta_{k+1} = \theta_k + \delta(\theta_k) \pmod{2\pi}. \tag{123}$$

Thus each numerical step is computed through the sequence

$$\theta_k \longmapsto \big(d(\theta_k), d'(\theta_k)\big) \longmapsto p(\theta_k) \longmapsto \sigma(\theta_k) \longmapsto \delta(\theta_k) \longmapsto \theta_{k+1}.$$

At every step we additionally monitor the radicand

$$\mathcal{R}(\theta) = 1 - d(\theta)\big(2 + d(\theta)\big)p(\theta)^2. \tag{124}$$

For both thickness profiles used below, $d(\theta) > 0$ and a direct substitution shows that

$$\mathcal{R}(\theta) > 0 \qquad \text{for every } \theta \in [0, 2\pi].$$

(A fine-grid evaluation gives $\min_\theta \mathcal{R} \approx 0.9102$ for the first profile and ≈ 0.1030 for the second one.) Hence the first-intersection branch (119) is real on the whole circle for both numerical examples.

As a basic consistency check, if $d'(\theta_*) = 0$, then $p(\theta_*) = 0$ and

$$\sigma(\theta_*) = d(\theta_*), \qquad \delta(\theta_*) = 0.$$

Hence

$$F(c(\theta_*)) = c(\theta_*),$$

in agreement with the fixed-point characterization of Theorem 7.1.

8.2 Validation of the First-Order Expansion

We first compare the exact unit-circle return map with the first-order angular displacement derived in Section 6.4.

Consider the thickness profile

$$d(\theta) = 0.5 + 0.2\cos(2\theta), \tag{125}$$

so that

$$d'(\theta) = -0.4\sin(2\theta). \tag{126}$$

We choose the initial condition

$$\theta_0 = 1. \tag{127}$$

For each iterate, the exact angular displacement $\delta_{\text{ex}}(\theta)$ is evaluated from (122), whereas the first-order prediction is

$$\delta_{\text{lin}}(\theta) = \frac{d(\theta)}{1 + d(\theta)} d'(\theta). \tag{128}$$

The first iterates of the exact return map are

$$\begin{aligned} 1 &\longmapsto 0.891275 \longmapsto 0.766007 \longmapsto 0.628467 \\ &\longmapsto 0.488793 \longmapsto 0.360872 \longmapsto 0.255671 \\ &\longmapsto 0.176381 \longmapsto \cdots. \end{aligned}$$

Table 1 compares the exact angular displacement with the first-order approximation. The trajectory itself is plotted in Figure 3.

The exact and first-order displacements have the same sign throughout the displayed trajectory. In particular, since $d'(\theta_k) < 0$, the return map moves toward decreasing values of θ, in agreement with the positive coefficient in (128).

Moreover, as the orbit approaches the critical point $\theta = 0$ (a local maximum of d), the difference between the exact and first-order displacements, after a slight initial increase over $k = 0, 1, 2$, decreases rapidly (Table 1). This is consistent with the estimate

$$\delta_{\text{ex}}(\theta) = \frac{d(\theta)}{1 + d(\theta)} d'(\theta) + O\big(|d'(\theta)|^2\big) \tag{129}$$

derived in Section 6.4.

For the displayed iterates, the radicand $\mathcal{R}(\theta_k)$ in (124) remains positive; its smallest value is approximately

$$0.910516.$$

Thus all reported steps belong to the real first-intersection branch of the exact return construction.

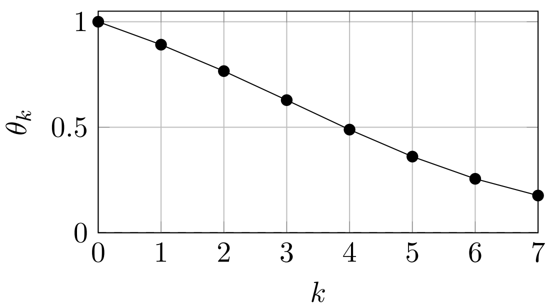

Figure 3. Exact iterates of the return map for $d(\theta) = 0.5 + 0.2\cos(2\theta)$ with initial condition $\theta_0 = 1$. The dashed line marks the critical point $\theta = 0$.

Table 1. Exact and first-order angular displacements for $d(\theta) = 0.5 + 0.2\cos(2\theta)$ with $\theta_0 = 1$.

k	θ_k	$d'(\theta_k)$	δ_{ex}	δ_{lin}	$\lvert\delta_{\text{ex}} - \delta_{\text{lin}}\rvert$
0	1.000000	-0.363719	-0.108725	-0.106995	0.001730
1	0.891275	-0.391066	-0.125268	-0.122839	0.002429
2	0.766007	-0.399699	-0.137540	-0.134604	0.002937
3	0.628467	-0.380459	-0.139674	-0.136848	0.002826
4	0.488793	-0.331660	-0.127921	-0.125891	0.002030
5	0.360872	-0.264278	-0.105202	-0.104122	0.001079
6	0.255671	-0.195739	-0.079290	-0.078839	0.000450
7	0.176381	-0.138197	-0.056472	-0.056311	0.000161

8.3 Validation of the Local Multiplier

We next test the local linearization derived in Section 7 using the thickness profile

$$d(\theta) = 0.6 + 0.4\cos(3\theta). \tag{130}$$

Its first two derivatives are

$$d'(\theta) = -1.2\sin(3\theta), \qquad d''(\theta) = -3.6\cos(3\theta). \tag{131}$$

The points

$$0, \qquad \frac{2\pi}{3}, \qquad \frac{4\pi}{3}$$

are local maxima of the thickness function, whereas

$$\frac{\pi}{3}, \qquad \pi, \qquad \frac{5\pi}{3}$$

are local minima.

We consider the maximum

$$\theta_* = 0.$$

At this point,

$$d(0) = 1, \qquad d''(0) = -3.6.$$

For the unit circle, the tangential preconditioning factor is

$$B_* = \frac{d(0)}{1 + d(0)} = \frac{1}{2}.$$

Hence the one-dimensional version of Theorem 7.3 gives

$$F'(\theta_*) = 1 + \frac{d(\theta_*)}{1 + d(\theta_*)} d''(\theta_*). \tag{132}$$

Therefore,

$$F'(0) = 1 + \frac{1}{2}(-3.6) = -0.8. \tag{133}$$

The negative multiplier predicts that sufficiently small perturbations of the fixed point change sign after each iteration, while their magnitude is asymptotically reduced by the factor 0.8.

Table 2. Validation of the local multiplier at the fixed point $\theta_* = 0$ for $d(\theta) = 0.6 + 0.4\cos(3\theta)$.

k	θ_k	θ_{k+1}	q_k
0	0.500000	-0.169402	-0.338804
1	-0.169402	0.133200	-0.786295
2	0.133200	-0.105476	-0.791861
3	-0.105476	0.083855	-0.795013
4	0.083855	-0.066823	-0.796891
5	-0.066823	0.053328	-0.798043
6	0.053328	-0.042596	-0.798760
7	-0.042596	0.034043	-0.799212
8	0.034043	-0.027217	-0.799497
9	-0.027217	0.021765	-0.799679
10	0.021765	-0.017408	-0.799795

To test this prediction, we apply the exact return-map algorithm of Section 8.1 with initial condition

$$\theta_0 = 0.5. \tag{134}$$

The resulting orbit begins

$$0.500000 \longmapsto -0.169402 \longmapsto 0.133200 \longmapsto -0.105476 \longmapsto 0.083855 \longmapsto -0.066823 \longmapsto 0.053328 \longmapsto \cdots.$$

For $\theta_k \neq 0$, define the observed local ratio

$$q_k := \frac{\theta_{k+1} - \theta_*}{\theta_k - \theta_*} = \frac{\theta_{k+1}}{\theta_k}. \tag{135}$$

Table 2 shows that the observed ratios approach the theoretical multiplier -0.8.

In particular, the values displayed in the last rows are already close to the linear prediction

$$\theta_{k+1} - \theta_* \approx -0.8\,(\theta_k - \theta_*).$$

The alternating signs of the computed iterates are consistent with the local behaviour of an attracting fixed point having a negative multiplier; they should not be interpreted as evidence of a period-two orbit. Over the displayed trajectory, the deviations from $\theta_* = 0$ decrease in magnitude while alternating in sign, in agreement with the exact local multiplier (133). The signed deviations are plotted in Figure 4.

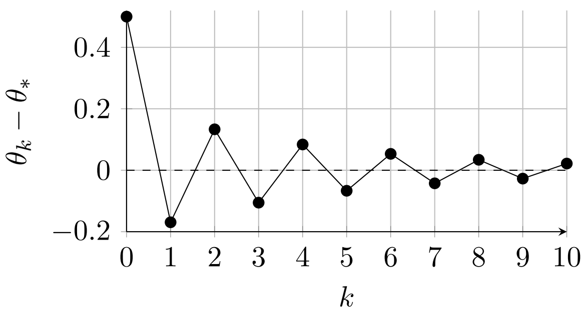

Figure 4. Signed deviation from the fixed point $\theta_* = 0$ for $d(\theta) = 0.6 + 0.4\cos(3\theta)$. The alternating sign and decreasing magnitude are consistent with the theoretical multiplier $F'(0) = -0.8$.

8.4 Reproducibility Details

All numerical values reported in this section were obtained by direct evaluation of the exact unit-circle return map (116)–(123). No numerical root-finding procedure and no first-order approximation were used to generate the iterates.

The computations were performed in double-precision floating-point arithmetic. At each iteration step, the quantities

$$d(\theta_k),\ d'(\theta_k),\ p(\theta_k),\ \mathcal{R}(\theta_k),\ \sigma(\theta_k),\ \delta(\theta_k)$$

were evaluated successively from the formulas given in Section 8.1.

Angles were represented in radians. Whenever necessary, the resulting angle was reduced modulo 2π. For computations near the fixed point $\theta_* = 0$, the locally continuous representative of the angular coordinate was used so that signed deviations from the fixed point remained meaningful.

The square-root branch in (119) was accepted only when

$$\mathcal{R}(\theta_k) = 1 - d(\theta_k)\big(2 + d(\theta_k)\big)p(\theta_k)^2 \geq 0. \tag{136}$$

For all iterates reported in Tables 1 and 2, this condition was satisfied.

For an iteration continued beyond the values displayed in the tables, the stopping criterion was

$$|\theta_{k+1} - \theta_k| < 10^{-12}. \tag{137}$$

The values printed in the tables are rounded to six decimal places, whereas all intermediate computations were performed without such rounding.

For the first example,

$$d(\theta) = 0.5 + 0.2\cos(2\theta), \qquad \theta_0 = 1,$$

the smallest value of the radicand among the displayed iterates is approximately

$$0.910516.$$

For the second example,

$$d(\theta) = 0.6 + 0.4\cos(3\theta), \qquad \theta_0 = 0.5,$$

the first displayed step gives the smallest radicand, approximately

$$0.107608.$$

Over the subsequent computed iterates, the radicand increases toward 1 as the deviations from $\theta_* = 0$ decrease.

The numerical data therefore arise directly from the exact geometric return construction and can be reproduced independently from the formulas stated above.

9 Regularity and Bi-Lipschitz Structure

The radial representation

$$\Phi(c) = c + d(c)\nu(c)$$

encodes the outer boundary entirely in terms of the convex core and the thickness function. In the preceding sections, only the regularity required for the return-map construction was imposed. We now record two basic structural consequences of this parametrization: the correspondence between the regularity of d and that of the outer boundary, and quantitative bi-Lipschitz bounds for Φ.

The discussion is deliberately restricted to the regularity properties needed for the geometric framework developed in this paper.

9.1 Regularity of the Thickness and the Outer Boundary

Under the standing assumptions of Section 2, the thickness function is locally Lipschitz by Proposition 3.1. We now record the corresponding higher-regularity statement under additional smoothness assumptions.

Proposition 9.1 (Regularity transfer)**.** *Let $m \geq 1$ and $0 \leq \alpha \leq 1$. Assume that ∂C is of class $C^{m+1,\alpha}$.*

1. *If*
$$d \in C^{m,\alpha}(\partial C),$$
then
$$\Phi(c) = c + d(c)\nu(c)$$
is of class $C^{m,\alpha}$. Moreover, Φ is a $C^{m,\alpha}$ parametrization of $\partial\Omega \setminus C$.

2. *Conversely, let $c_0 \in \partial C$ and $x_0 = \Phi(c_0)$. If $\partial\Omega$ is of class $C^{m,\alpha}$ near x_0 and the radial intersection is transverse,*
$$\langle n(x_0), \nu(c_0)\rangle \neq 0,$$
then d is of class $C^{m,\alpha}$ in a neighbourhood of c_0.

Proof. For the first assertion, the regularity of ∂C implies that the outward normal field

$$\nu : \partial C \longrightarrow \mathbb{S}^{N-1}$$

is of class $C^{m,\alpha}$. Hence

$$\Phi(c) = c + d(c)\nu(c)$$

is $C^{m,\alpha}$ whenever d is $C^{m,\alpha}$.

It remains to verify that the parametrization is nondegenerate. For $v \in T_c\partial C$, equation (18) gives

$$D\Phi(c)[v] = \big(I - d(c)S_c\big)v + \langle \nabla_{\partial C} d(c), v\rangle \nu(c).$$

The tangential and normal components are orthogonal. Therefore, if

$$D\Phi(c)[v] = 0,$$

then necessarily

$$\big(I - d(c)S_c\big)v = 0.$$

For a convex core, the eigenvalues of $I - d(c)S_c$ are

$$1 + d(c)\kappa_i(c) > 0,$$

so the operator is invertible and hence $v = 0$. Thus $D\Phi(c)$ has full rank.

By Proposition 2.3, Φ is already globally bijective from ∂C onto $\partial\Omega \setminus C$. The local inverse-function theorem therefore shows that Φ provides a $C^{m,\alpha}$ parametrization of the outer boundary.

For the converse, choose a local $C^{m,\alpha}$ defining function ρ for $\partial\Omega$ near x_0, so that

$$\partial\Omega = \{\rho = 0\}, \qquad \nabla\rho(x_0) \neq 0.$$

Let $c = c(y)$ be a local parametrization of ∂C near c_0 and define

$$G(y,t) = \rho\big(c(y) + t\nu(c(y))\big). \tag{138}$$

By construction,

$$G(y, d(c(y))) = 0.$$

At the point corresponding to c_0,

$$\partial_t G(y_0, d(c_0)) = \langle \nabla\rho(x_0), \nu(c_0)\rangle\,. \tag{139}$$

Since $\nabla\rho(x_0)$ is normal to $\partial\Omega$ at x_0, the transversality assumption implies

$$\partial_t G(y_0, d(c_0)) \neq 0.$$

The classical implicit-function theorem therefore yields a unique $C^{m,\alpha}$ solution

$$t = d(c(y))$$

near y_0. Hence d is $C^{m,\alpha}$ near c_0. □

Remark 9.2. The converse implication uses the radial transversality explicitly. It does not rely on assuming in advance that the inverse of the radial map is smooth. This avoids the circular inverse-map argument that can arise if regularity of Φ^{-1} is used before nondegeneracy of Φ has been established.

9.2 Bi-Lipschitz Bounds for the Radial Map

The radial parametrization admits global quantitative bounds that follow directly from convex projection. In particular, no smallness condition involving the thickness or the curvature of the convex core is required.

Let

$$L_d := \mathrm{Lip}(d), \qquad L_\nu := \mathrm{Lip}(\nu), \qquad d_{\max} := \|d\|_{L^\infty(\partial C)}.$$

Under the standing assumptions, these quantities are finite: ν is Lipschitz because ∂C is of class $C^{1,1}$, while Proposition 3.1, together with compactness of ∂C, gives a global Lipschitz constant for d.

Proposition 9.3 (Global bi-Lipschitz estimate)**.** *Let $\Omega \in \mathcal{O}_C$ and let*

$$\Phi(c) = c + d(c)\nu(c).$$

Then for every $c_1, c_2 \in \partial C$,

$$|c_1 - c_2| \leq |\Phi(c_1) - \Phi(c_2)| \leq \big(1 + L_d + d_{\max}L_\nu\big)|c_1 - c_2|. \tag{140}$$

Consequently,

$$\Phi : \partial C \longrightarrow \partial\Omega \setminus C$$

is bi-Lipschitz. Moreover, its inverse satisfies

$$\mathrm{Lip}(\Phi^{-1}) \leq 1. \tag{141}$$

Proof. By Proposition 2.3,

$$\Phi^{-1} = P_C\big|_{\partial\Omega\setminus C}.$$

Since the metric projection onto a closed convex set is non-expansive,

$$|P_C(x_1) - P_C(x_2)| \leq |x_1 - x_2|$$

for all $x_1, x_2 \in \mathbb{R}^N$.

Taking

$$x_i = \Phi(c_i), \qquad i = 1, 2,$$

and using

$$P_C(\Phi(c_i)) = c_i,$$

gives

$$|c_1 - c_2| \leq |\Phi(c_1) - \Phi(c_2)|. \tag{142}$$

For the upper bound, write

$$\begin{aligned} \Phi(c_1) - \Phi(c_2) &= c_1 - c_2 + d(c_1)\nu(c_1) - d(c_2)\nu(c_2) \\ &= c_1 - c_2 + \big(d(c_1) - d(c_2)\big)\nu(c_1) \\ &\quad + d(c_2)\big(\nu(c_1) - \nu(c_2)\big). \end{aligned} \tag{143}$$

Hence

$$\begin{aligned} |\Phi(c_1) - \Phi(c_2)| &\leq |c_1 - c_2| + |d(c_1) - d(c_2)| \\ &\quad + d(c_2)|\nu(c_1) - \nu(c_2)| \\ &\leq \big(1 + L_d + d_{\max}L_\nu\big)|c_1 - c_2|. \end{aligned} \tag{144}$$

Combining (142) and (144) proves (140).

Finally, the lower bound is equivalent to

$$|\Phi^{-1}(x_1) - \Phi^{-1}(x_2)| \leq |x_1 - x_2|,$$

which proves (141). □

Remark 9.4. The estimate (140) does not require a condition of the form

$$L_d + d_{\max}L_\nu < 1.$$

The lower Lipschitz bound follows instead from the convexity of C and the non-expansiveness of the metric projection. Thus the bi-Lipschitz property is a structural consequence of the global radial representation established in Proposition 2.3, rather than a perturbative smallness result.

10 Discussion and Outlook

The construction developed in this paper shows that the geometric normal properties of the class $\mathcal{O}_C$ naturally generate a discrete dynamical system on the boundary of the convex core. The essential mechanism is the geometric round-trip

$$c \longmapsto \Phi(c) = c + d(c)\nu(c) \longmapsto F(c),$$

where the outward radial displacement is determined by the normal geometry of ∂C, whereas the return step is determined by the inward normal geometry of $\partial\Omega$.

The analysis reveals that these two normal structures are coupled through the thickness function. In particular, the first-order return displacement is governed by the positive tangential operator

$$B_c = d(c)\big(I - d(c)S_c\big)^{-1},$$

so that, near a critical point of the thickness,

$$F(c) - c = B_c\nabla_{\partial C}d(c) + O\big(|\nabla_{\partial C}d(c)|^2\big).$$

Thus curvature of the convex core enters directly into the leading-order dynamics through an anisotropic preconditioning of the thickness gradient.

This geometric structure also clarifies the local equilibrium theory. At differentiability points, critical points of the thickness are precisely the fixed points of the return map. Under the additional smoothness assumptions used in Section 7, this equivalence holds pointwise, and the derivative at a critical point is

$$DF(c_*) = I + B_*H_*,$$

where

$$B_* = d_*\big(I - d_*S_*\big)^{-1}$$

and H_* is the Hessian operator of the thickness at c_*. The local stability of a fixed point therefore depends on the interaction between the second-order variation of the thickness and the curvature of the convex core, rather than on the Hessian of d alone.

The numerical examples of Section 8 provide direct checks of this local theory using the exact return geometry on the unit circle. They confirm both the first-order displacement and the local multiplier predicted by the linearization. Their purpose is validation of the geometric formulas rather than a classification of the global dynamics.

The regularity results of Section 9 complement this dynamical picture. The radial parametrization transfers regularity between the thickness function and the outer boundary, while convex metric projection gives a global bi-Lipschitz control of the radial map. In particular, this control does not require a perturbative smallness condition.

The present paper is intentionally limited to these foundational properties. Several questions arising naturally from the return construction require a separate analysis. These include the global behaviour of the iterates, possible monotonicity or Lyapunov structures, the existence and stability of nontrivial periodic orbits, and the relation between the critical-point structure of the thickness and the topology of ∂C. A continuous-time limit of the return dynamics would likewise require an appropriate scaling and a separate consistency analysis.

The framework developed here provides the geometric starting point for such investigations. In particular, the operator

$$d(c)\big(I - d(c)S_c\big)^{-1}$$

identifies the interaction between thickness and curvature that must be retained in any subsequent dynamical or topological analysis of the return map.

11 Conclusion

We have developed the geometric and analytical foundations of the return map associated with domains in the class $\mathcal{O}_C$. Starting from the radial representation

$$\Phi(c) = c + d(c)\nu(c),$$

and the reciprocal map defined by inward normal rays from the outer boundary, we obtained a discrete return dynamics

$$F = \pi \circ \Phi : \partial C \longrightarrow \partial C.$$

The exact normal geometry of the radial parametrization leads to the local quadratic-remainder formula

$$F(c) - c = d(c)\big(I - d(c)S_c\big)^{-1}\nabla_{\partial C} d(c) + O\big(|\nabla_{\partial C} d(c)|^2\big).$$

Thus the leading-order return displacement is a curvature-preconditioned gradient step whose metric dependence is determined by the geometry of the convex core.

We showed that, at differentiability points, the fixed points of the return map coincide with the critical points of the thickness function. Under the corresponding smoothness assumptions, this equivalence holds pointwise. The derivative at a critical point c_* is

$$DF(c_*) = I + d_*\big(I - d_*S_*\big)^{-1}H_*,$$

which yields a local stability criterion through the interaction between the Hessian of the thickness and the curvature of ∂C.

The unit-circle computations provide reproducible checks of the first-order displacement and of the local multiplier predicted by the linearization. In addition, the radial parametrization gives a direct regularity correspondence between the thickness function and the outer boundary and satisfies global bi-Lipschitz bounds derived from convex metric projection.

These results establish the return map as a geometrically defined discrete dynamical system whose local behaviour is controlled by the coupled effects of thickness and curvature. They provide the foundational framework for subsequent investigations of global dynamics, periodic behaviour, convergence mechanisms, and the topological structure of the thickness landscape.

Data Availability Statement

The data used to support the findings of this study are available from the corresponding author upon request. All numerical results in Section 8 can be reproduced from the explicit formulas stated there; no external datasets were used.

Funding

This work was supported without any funding.

Conflicts of Interest

Mohamed El Morsalani is affiliated with the QWave Consult, Ostfildern, Germany. The authors declare that this affiliation had no influence on the study design, data collection, analysis, interpretation, or the decision to publish, and that no other competing interests exist.

AI Use Statement

The authors declare that ChatGPT-5 was used for drafting and language editing of the manuscript. The authors have carefully reviewed, revised, and verified the AI-assisted output and take full responsibility for the content of the manuscript.

Ethical Approval and Consent to Participate

Not applicable.

References

[1] Schneider, R. (2014). *Convex bodies: The Brunn-Minkowski theory* (2nd expanded ed.; Encyclopedia of Mathematics and Its Applications, vol. 151). Cambridge University Press. [CrossRef]

[2] Henrot, A., & Pierre, M. (2005). *Variation et optimisation de formes: Une analyse géométrique* (Mathématiques & Applications, vol. 48). Springer. [CrossRef]

[3] Sokolowski, J., & Zolesio, J.-P. (1992). *Introduction to shape optimization: Shape sensitivity analysis* (Springer Series in Computational Mathematics, vol. 16). Springer. [CrossRef]

[4] Plotnikov, P. I., & Sokolowski, J. (2023). Geometric aspects of shape optimization. *The Journal of Geometric Analysis*, *33*(7), 206. [CrossRef]

[5] Welker, K. (2021). Suitable spaces for shape optimization. *Applied Mathematics & Optimization*, *84*, 869-902. [CrossRef]

[6] Barkatou, M. (2002). Some geometric properties for a class of non-Lipschitz domains. *New York Journal of Mathematics*, *8*, 189-213. https://ftp.gwdg.de/pub/misc/EMIS/journals/NYJM/j/2002/8-13.pdf

[7] Ambrosio, L., & Mantegazza, C. (1998). Curvature and distance function from a manifold. *The Journal of Geometric Analysis*, *8*(5), 723-748. [CrossRef]

[8] Lytchak, A. (2024). A note on subsets of positive reach. *Mathematische Nachrichten*, *297*(3), 932-942. [CrossRef]

[9] Hug, D., & Santilli, M. (2022). Curvature measures and soap bubbles beyond convexity. *Advances in Mathematics*, *411*, 108802. [CrossRef]

[10] Boumal, N. (2023). *An introduction to optimization on smooth manifolds*. Cambridge University Press. [CrossRef]

[11] do Carmo, M. P. (1976). *Differential geometry of curves and surfaces*. Prentice-Hall. https://docenti.ing.unipi.it/griff/files/dC.pdf

[12] Rockafellar, R. T. (1970). *Convex analysis*. Princeton University Press. https://www.jstor.org/stable/j.ctt14bs1ff

Dr. Mohammed Barkatou is a mathematician at Chouaïb Doukkali University in Morocco. He holds a Ph.D. in Mathematics and Applications from the University of Franche-Comté (France). His research focuses on shape optimization, free boundary problems, calculus of variations, and discrete optimization. He has supervised 5 doctoral theses. (Email: barkatou.m@ucd.ac.ma)

Dr. Mohamed El Morsalani is a mathematician, researcher, and quantum technologies consultant at QWave Consult in Ostfildern, Germany. He holds a PhD in mathematics and has more than two decades of professional experience in quantitative finance, risk analysis, and advanced technologies. His mathematical research focuses on geometric analysis and dynamical systems, particularly the geometric and dynamical analysis of return maps in structured classes of domains. In parallel, his research in quantum technologies addresses quantum cryptography, post-quantum cryptography, open quantum dynamics, and the geometric foundations of quantum information, including mixed-state geometry and holonomy-based secrecy frameworks. His work is driven by a broader interest in uncovering and analysing hidden geometric and dynamical structures across both classical and quantum systems. (Email: mohamed.elmorsalani@qwave-consult.eu)